

Different scenarios of dynamical chiral symmetry breaking in the interacting instanton liquid model via flavor symmetry breaking

Yamato Suda¹ and Daisuke Jido¹

¹*Department of Physics, Institute of Science Tokyo,
2-12-1 Ookayama, Meguro, Tokyo 152-8551, Japan*

(Dated: April 29, 2025)

We investigate a type of dynamical chiral symmetry breaking (D χ SB) for various current quark masses using the interacting instanton liquid model. The type of D χ SB is classified based on the sign of the second derivative of the free energy density with respect to the quark condensate at the origin. We perform numerical simulations of the interacting instanton liquid model with the flavor SU(2) symmetric and (2+1)-flavor quarks. We find that the curvature is negative in the SU(2) case. This means the ordinary type of D χ SB. In contrast, in the (2+1)-flavor case, a positive curvature is observed when the strange quark mass is as small as those of the up and down quarks. This suggests that the anomaly-driven type of D χ SB can occur under the approximate flavor SU(3) symmetry. As the strange quark mass increases, the curvature gradually decreases and becomes negative when the strange quark mass is approximately three times larger than those of the light quarks. This difference can be understood in terms of the 't Hooft vertex which induces a six-quark interaction in the $N_f = 3$ case and does a four-quark interaction in the $N_f = 2$ case. Our results might indicate that the ratio between the strange and light quark masses plays a crucial role in understanding the microscopic relationship between D χ SB and the anomaly effect.

I. INTRODUCTION

Understanding the nature of dynamical chiral symmetry breaking (D χ SB) in the vacuum of strong interaction is one of the most important subjects in hadron physics [1]. The fundamental theory of strong interaction, quantum chromodynamics (QCD), is invariant under the chiral transformation at the Lagrangian level in the chiral limit. Due to the non-perturbative dynamics of quarks and gluons, quark and anti-quark are condensed in the vacuum, leading to the dynamical breaking of chiral symmetry as

$$SU(N_f)_L \times SU(N_f)_R \times U(1)_A \rightarrow SU(3)_V. \quad (1)$$

The $U(1)_A$ symmetry is also broken by a quantum anomaly initially identified by Adler, Bell and Jackiw [2, 3]. Due to this anomaly, called the axial anomaly, the singlet η' meson acquires relatively large mass than the other Nambu–Goldstone bosons [4]. D χ SB is responsible not only for the most of the hadron mass generation, but also for the non-trivial vacuum structure of strong interaction.

The chiral effective theories, such as the chiral perturbation theory, the linear sigma model and the Nambu–Jona-Lasinio model, are based on the structure of symmetry and its breaking pattern [5–8]. These successes are often regarded as being independent of the details of how chiral symmetry is broken in the vacuum, in other words, independent of the microscopic mechanism behind it. However, it remains an open and interesting question whether the specific dynamics of D χ SB might leave observable remnants in hadron properties.

In fact, the authors of Ref. [9] suggested that the type of dynamics inducing D χ SB in vacuum could affect not only the vacuum structure but also the hadron

spectrum emerging from it. The authors investigated systematically the model parameter dependence of the type of D χ SB and the hadron spectra by using the chiral effective theories with the $U(1)_A$ anomaly effect via the Kobayashi–Maskawa–'t Hooft (KMT) term [10–16]. They confirmed the ordinary type of D χ SB in which chiral symmetry is dynamically broken when the four-quark coupling parameter exceeds its critical value in the three-flavor linear sigma model and the Nambu–Jona-Lasinio (NJL) model. Additionally, they showed that chiral symmetry can be broken with a sufficiently large contribution from the $U(1)_A$ anomaly effect, even if the four-quark coupling is not strong enough to exceed its critical value. Calculating the hadron masses under both situations of the ordinary and anomaly-driven types of D χ SB, they found that the sigma meson, which is introduced as the chiral partner of the pion, obtains a heavier mass $m_\sigma > 800$ MeV for the former case and a lighter mass $m_\sigma < 800$ MeV for the latter case [9].

In the previous study [9], the criterion to identify the type of D χ SB is based on the specific model parameters g_S and g_D that represent the four-quark coupling and the strength of the $U(1)_A$ anomaly effect, respectively. More specifically, the ordinary type of D χ SB is characterized by a nonzero quark condensate in vacuum with $g_S > g_S^{\text{crit}}$. The specific value of the critical coupling g_S^{crit} is determined by the cutoff scheme used. While the anomaly-driven type of D χ SB is characterized by $\langle \bar{q}q \rangle \neq 0$ in vacuum even though $g_S < g_S^{\text{crit}}$. That is possible with sufficiently large negative value of g_D . This result suggests that the type of D χ SB—whether it is driven predominantly by the four-quark interactions or by the anomalous $U(1)_A$ dynamics—may leave distinguishable footprints in the hadron spectrum. In particular, the mass of the σ meson, often regarded as a manifestation of the chiral order parameter, could serve as a probe of

the underlying mechanism of $D\chi SB$.

In Ref. [17], we investigated whether such different types of $D\chi SB$ can be realized in other models than those used in Ref. [9]. We firstly defined the criterion to identify the type of $D\chi SB$ by the sign of the curvature, which is given by a second derivative of the energy density of the vacuum with respect to the quark condensate at its origin. When this curvature has negative or positive value, the realizing $D\chi SB$ is referred to as the ordinary type or the anomaly-driven one. This is a generalized criterion of that discussed in Ref. [9]. In fact, by including the anomaly term in the three-flavor NJL model and using coupling constants that realize the ordinary and anomaly-driven types of $D\chi SB$, one can confirm that the curvature reproduces negative and positive values, respectively [17].

In our previous study [17], we then performed numerical simulations of the interacting instanton liquid model (IILM) and evaluated the curvature in IILM with the flavor $SU(3)$ symmetric quarks and in the quenched calculation. The previous work concluded that IILM with the flavor $SU(3)$ symmetric quarks exhibits the anomaly-driven type of $D\chi SB$, while the quenched calculation shows the ordinary type of $D\chi SB$ [17].

This difference can be understood from the perspective of quark-instanton interactions mediated by the so-called 't Hooft vertex [13, 18–20]. In the quenched calculation, the quark determinant is omitted from the partition function. This removes the dynamical interaction between quarks and instantons. As a result, the multi-fermion vertex induced by instantons that involves $2N_f$ quark legs and brings the effects of the $U(1)_A$ anomaly does not arise in the quenched calculation. This leads to a suppression of anomaly effects. Thus, the $D\chi SB$ mechanism is found to be of the ordinary type.

In contrast, IILM with the flavor $SU(3)$ symmetric quarks includes the full quark determinant that provides the dynamical quark-instanton interaction. The resulting 't Hooft vertex in this case is a six-quark interaction. This corresponds to the KMT term in chiral effective theories. Since this interaction originates from the $U(1)_A$ anomaly, the effect of the axial anomaly is included in this calculation. Therefore, in the flavor $SU(3)$ symmetric IILM, the anomaly-driven type of $D\chi SB$ is naturally understood. From this, we anticipate that the presence of three quarks with the flavor $SU(3)$ symmetry may play an important role in inducing the anomaly-driven type of $D\chi SB$.

In nature, the u and d quarks have nearly equal masses, $m_u \approx m_d$, while the s quark is significantly heavier, $m_s \gg m_u, m_d$ [21]. Therefore, the flavor symmetry that more closely reflects the physical situation is $SU(2)$ and it is nontrivial to extrapolate our conclusions in the flavor $SU(3)$ symmetric and quenched calculations to the physical case, where the flavor $SU(3)$ symmetry is slightly broken due to the mass difference among the u, d and s quarks. This implies that further investigation is necessary to understand how the anomaly-driven type of

$D\chi SB$ is physically realized.

In this study, we investigate the dependence of the type of $D\chi SB$ on the number of quark flavors using IILM with the flavor $SU(2)$ symmetric and $(2+1)$ -flavor quarks. The aim of this study is to clarify how the type of $D\chi SB$ changes as we move from the flavor $SU(3)$ symmetric system to the flavor $SU(2)$ symmetric one by increasing the strange quark mass. This can be one of the clues to understanding the nature of $D\chi SB$ occurring in the vacuum of strong interaction.

This paper is organized as follows. In Sect. II, we demonstrate the formulation of IILM and computational details used in this study. In Sect. III, we show the results of the flavor $SU(2)$ and $(2+1)$ -flavor calculations with various quark masses. In Sect. IV, we summarize this paper.

II. METHODOLOGY

In this section, we will explain the model used in this study and the computational procedures for measurements relevant to our evaluations. In addition, we will describe how to extract the curvature from those quantities in the numerical simulation of IILM.

A. Partition function

We begin with the partition function of IILM in the four-dimensional Euclidean space-time given by Ref. [26]:

$$Z = \frac{1}{N_+!N_-!} \int \prod_{i=1}^{N_++N_-} [d\Omega_i f(\rho_i)] \exp(-S_{\text{int}}) \times \prod_f \text{Det}(\not{D} + m_f), \quad (2)$$

where the number of instantons and anti-instantons are denoted as N_{\pm} . The path integral measure is represented by $d\Omega_i = dU_i d^4z_i d\rho_i$, which consists of the collective coordinates, such as color orientation U , position z , and size ρ of an instanton or anti-instanton labeled by i . The semiclassical instanton amplitude $f(\rho)$ as a function of the instanton size ρ depends on the number of colors $N_c = 3$ and of flavors N_f via the β functions. This is originally calculated by 't Hooft and extended to $SU(N_c)$ group by Bernard [13, 24]. In the calculation of $f(\rho)$, a scale parameter Λ is introduced [25]. Its explicit form is given in Appendix A. All quantities in this study are computed in units of the scale parameter Λ .

The action S_{int} accounts for the interaction between instantons. According to Ref. [26], we approximate it by a sum of a purely two-body interaction $S_{\text{int}} = (1/2) \sum_{l \neq m} S_{\text{int}}^{(2)}(l, m)$ for all possible combinations of instantons and anti-instantons. The quark determinant $\text{Det}(\not{D} + m_f)$ arises from the path integral of degrees of

freedom of quarks with a current mass m_f . This introduces a nonlocal interaction among instantons. The details for these interactions are described in Sect. II B.

The dynamics of instantons and anti-instantons described by the partition function in Eq. (2) can be simulated by using standard Monte Carlo techniques, such as the Metropolis algorithm and the HMC algorithm, originally developed for simulations of statistical mechanics of atoms or molecules [29] and lattice field theory [30]. In the present case, we fix a total number of instantons and anti-instantons, $N \equiv N_+ + N_- = 16 + 16 = 32$. We then perform a simulation of ILM according to Eq. (2) at a given instanton density, $n \equiv N/V$, by adjusting a four-volume of the system V . To investigate the instanton density dependence of measurements, we vary the four-volume V while keeping N fixed.

In this simulation, the remaining input parameters are current quark masses, $m_f = (m_u, m_d, m_s)$. In practice, the current quark masses are specified in units of Λ at the beginning of the simulation. Once Λ is determined for given quark masses m_f , the quantities given in units of Λ can be converted into physical units such as MeV and fm.

We determine the value of the scale parameter Λ such that the free energy density has its minimum at an instanton density of $n = 1 \text{ fm}^{-4}$, following Ref. [26]. The definition of the free energy density is given in Sect. II C.

B. Interactions

The two-body interaction $S_{\text{int}}^{(2)}(l, m) = S[A_\mu(l, m)] - 2S_0$ is calculated by inserting the instanton-anti-instanton gauge potential. Here, the single instanton action is denoted as $S_0 = 8\pi^2/g^2$. For this potential, we use the streamline configuration [27]. In practice, we introduce a phenomenological short range repulsive core in both the instanton-instanton and anti-instanton-anti-instanton interactions. This includes a parameter A that controls the strength of the core. We use $A = 128$ that is tuned so as to make the ensemble not as dilute as that suggested by phenomenology [26]. The explicit expression of S_{int} is given in Appendix. B.

The quark determinant for each quark flavor f can be written as a product of determinants over high and low momentum parts [25]:

$$\begin{aligned} \text{Det}(\mathcal{D} + m_f) &\equiv \text{Det}_{\text{high}}(\mathcal{D} + m_f) \text{Det}_{\text{low}}(\mathcal{D} + m_f) \\ &\equiv \left(\prod_{i=1}^N 1.34\rho_i \right) \text{Det}_{\text{I}, \bar{\text{I}}}(-iT + m_f \mathbf{1}), \end{aligned} \quad (3)$$

where the first factor, the high momentum part, is given as a product of contributions from the background field of individual instantons, whereas the low momentum part responsible for the quark zero-mode in the instanton and anti-instanton backgrounds is calculated exactly. Here, T represents the overlap matrix with a size of $N \times N$. This

matrix is spanned by the quark zero-mode wave functions associated with the instanton or the anti-instantons. Thus, the determinant $\text{Det}_{\text{I}, \bar{\text{I}}}$ is understood as an operation carried out over the space spanned by the quark zero-modes of size $N \times N$. The explicit expression of T is also given in Appendix. B.

For the flavor SU(2) symmetric case, we use $N_f = 2$ in the calculation of $f(\rho)$, while for the case of the (2+1)-flavor quarks, we use $N_f = 3$ for that. In addition, we treat the quark determinant part of Eq. (2) as

$$\prod_f \text{Det}(\mathcal{D} + m_f) = [\text{Det}(\mathcal{D} + m_q)]^{N_f}, \quad (4)$$

for the flavor symmetric cases such as the flavor SU(3) and SU(2) calculations, and

$$\prod_f \text{Det}(\mathcal{D} + m_f) = \prod_{f=q,s} \text{Det}(\mathcal{D} + m_f) \quad (5)$$

for the (2+1)-flavor case. In this work, we assume that the masses of the u and d quarks are equal and refer them as $m_q \equiv m_u = m_d$. The s quark mass is denoted as m_s .

This quark determinant for a single flavor originates from the path integral over the fermionic degrees of freedom for that flavor [28]. Thus, the single-flavor determinant corresponds to a two-quark vertex in the effective Lagrangian of the instanton model discussed in Ref. [20]. This implies that the determinant structure in Eq. (4) can be interpreted as including up to four-quark interactions for $N_f = 2$. In contrast, the determinant form in Eq. (5) may correspond to a six-quark effective interaction that introduces the effect of the axial anomaly to the system for $N_f = 3$. This is the significant difference between the flavor SU(2) symmetric case and the (2+1)-flavor case in this model.

C. Measurements

The free energy density F is given by logarithm of the partition function in Eq. (2), divided by the volume V :

$$F = -\frac{1}{V} \ln Z. \quad (6)$$

In the following, we refer this simply as the free energy. The value of F is calculated at each instanton density n for fixed quark masses, (m_q, m_q) for the flavor SU(2) symmetric calculations and (m_q, m_q, m_s) for the (2+1)-flavor ones. To compute the free energy, we use the thermodynamics integration method, which was first applied to this framework by Schäfer and Shuryak in Ref. [26].

The quark condensate for a single flavor f of mass m_f is evaluated as the expectation value of the traced quark propagator at the same coordinate:

$$\begin{aligned} \langle \bar{\psi}_f \psi_f \rangle &\approx -\lim_{y \rightarrow x} \frac{1}{Z} \int D\Omega e^{-S_{\text{int}}} \prod_{f'} \text{Det}(\mathcal{D} + m_{f'}) \\ &\quad \times \text{Tr} [S^{\text{ZM}}(x, y; m_f)], \end{aligned} \quad (7)$$

where we write $D\Omega \equiv \prod_i^N [d\Omega_i f(\rho_i)]$ in short, and we approximate the full quark propagator $S(x, y; m_f)$ by the zero-mode propagator $S^{\text{ZM}}(x, y; m_f)$ [25]. The trace Tr is performed over the Dirac and color indices. The value of $\langle \bar{\psi}_f \psi_f \rangle$ is also calculated at each instanton density n once we specify the quark masses. The explicit form of the zero-mode propagator is given by

$$S^{\text{ZM}}(x, y; m_f) = \sum_{I, J} \left[\psi_{0, I}(x) [(-iT + m_q)^{-1}]_{I, J} \psi_{0, J}^\dagger(y) \right] \quad (8)$$

Here, $\psi_{0, I}(x)$ is the quark zero-mode wave function in the instanton background and T is the overlap matrix defined in Eq. (3). For further details, see Refs. [17, 28]. We simply write the u and d quark condensates by $\langle \bar{q}q \rangle \equiv \langle \bar{\psi}_u \psi_u \rangle = \langle \bar{\psi}_d \psi_d \rangle$, and refer this as light quark condensate, whereas we explicitly denote the flavor for the s quark condensate as $\langle \bar{s}s \rangle \equiv \langle \bar{\psi}_s \psi_s \rangle$.

By computing the free energy and the quark condensate at each instanton density, for given quark masses we obtain the set of measurements as a function of the instanton density as $(F_j, \langle \bar{q}q \rangle_j)$ for the flavor SU(2) symmetric and $(F_j, \langle \bar{q}q \rangle_j, \langle \bar{s}s \rangle_j)$ for the (2+1)-flavor calculations, where index j labels the instanton density.

To evaluate the curvature for given quark masses m_f , we perform the polynomial regression on the dataset $(F_j, \langle \bar{q}q \rangle_j)$ for both cases of the flavor SU(2) symmetric and the (2+1)-flavor. The polynomial model that to be fitted is given by

$$F = C_0 + C_1 \langle \bar{q}q \rangle + \frac{1}{2} C_2 \langle \bar{q}q \rangle^2 + \cdots + \frac{1}{k!} C_k \langle \bar{q}q \rangle^k, \quad (9)$$

with the polynomial order k . We vary the order k from 1 to 3 in this study to investigate systematic variation. We will show only the results of $k = 3$ in Sect. III because we find no qualitative difference between the results of $k = 2$ and 3. In the following, we simply refer to the coefficient C_2 as curvature.

As we have mentioned in Sect. I, one of the key characteristics to classify the type of D χ SB is the sign of this curvature. We define the anomaly-driven type of chiral symmetry breaking as occurring in the vacuum when the curvature is positive, and the ordinary type of chiral symmetry breaking as occurring in the vacuum when the curvature is negative.

D. Computational setups

We perform the numerical simulations of IILM with the flavor SU(2) symmetric and (2+1)-flavor quarks. For the flavor SU(2) symmetric calculation, we prepare six sets of simulations at different quark masses with setting the u and d quarks to have equal mass m_q . For the (2+1)-flavor calculation, we prepare 37 sets of simulations at different quark masses where the u and d quarks have equal mass m_q while the s quark is heavier; $m_q < m_s$.

TABLE I. Values of m_q in units of Λ for the simulations of IILM with the flavor SU(2) symmetric quarks. Values of the scale parameter Λ are determined following the procedure in the text. Values of m_q in units of MeV are calculated by using these values of Λ .

Sets	B1	B2	B3	B4	B5	B6
m_q (Λ)	0.05	0.08	0.10	0.15	0.18	0.20
Λ (MeV)	331	322	325	320	316	316
m_q (MeV)	17	26	32	48	57	63

The values of m_q and m_s in units of Λ are summarized in Table. I for $N_f = 2$ and Table. II for $N_f = 2 + 1$.

In performing those simulations, we use the standard Metropolis algorithm for updating the color orientation U_i , and we use the HMC algorithm for updating the size ρ_i and position z_i of an i th instanton [31–33]. In scanning the instanton density dependence of the measurements, we calculate with 72 different instanton densities. One simulation at a given instanton density and quark masses consists of 5000 configurations that are generated after 1000 initial sweeps.

III. RESULTS

We focus on the curvature C_2 obtained from the $\langle \bar{q}q \rangle$ dependence of F . In Sect. III A, we will present the results for the flavor SU(2) symmetric case and compare it to the flavor SU(3) symmetric case obtained in our previous study [17]. In Sect. III B, we will show the results for the (2+1)-flavor calculations. Finally, in Sect. III C, we will examine the difference between the flavor SU(3) and SU(2) symmetric cases by analyzing the (2+1)-flavor results.

A. The flavor SU(2) symmetric calculation

In Fig. 1, we show the free energy as a function of the instanton density that is computed in the flavor SU(2) symmetric IILM. The free energy decreases as the instanton density increases and it increases beyond its minimum. This behavior clearly shows the attraction among instantons at the dilute density and the repulsive behavior in the dense density. An increase in the current quark mass reduces the minimum of the free energy. These attractive and repulsive interactions at the dilute and dense instanton density, and the reduction of the free energy are quantitatively agree with the results in the previous studies [17, 26].

In Fig. 2, we present the light quark condensate as a function of the instanton density. The absolute value of the quark condensate monotonically increase as the instanton density increases. At the vacuum of $n = 1 \text{ fm}^{-4}$, the quark condensate takes about $\langle \bar{q}q \rangle = (-207 \text{ MeV})^3$ independent of the current quark mass. This value

TABLE II. Quark masses $m_f = (m_q, m_q, m_s)$ in units of Λ for the simulations of ILM with the (2+1)-flavor quarks. Values of Λ and (m_q, m_s) in units of MeV are calculated in the same way as in Table I.

Sets	C1	C2	C3	C4	C5	C6	
(m_q, m_s) (Λ)	(0.08, 0.10)	(0.08, 0.15)	(0.08, 0.30)	(0.08, 0.60)	(0.08, 0.90)	(0.08, 1.2)	
Λ (MeV)	394	379	364	336	326	314	
(m_q, m_s) (MeV)	(31, 39)	(30, 57)	(29, 109)	(27, 202)	(26, 293)	(25, 377)	
Sets	D1	D2	D3	D4	D5	D6	D7
(m_q, m_s) (Λ)	(0.10, 0.15)	(0.10, 0.30)	(0.10, 0.45)	(0.10, 0.60)	(0.10, 0.75)	(0.10, 0.90)	(0.10, 1.2)
Λ (MeV)	372	358	349	338	331	322	319
$(m_q, , m_s)$ (MeV)	(37, 56)	(36, 108)	(35, 157)	(34, 203)	(33, 249)	(32, 290)	(32, 383)
Sets	E1	E2	E3	E4	E5	E6	
(m_q, m_s) (Λ)	(0.15, 0.20)	(0.15, 0.30)	(0.15, 0.45)	(0.15, 0.60)	(0.15, 0.90)	(0.15, 1.2)	
Λ (MeV)	365	353	335	329	322	310	
(m_q, m_s) (MeV)	(55, 73)	(53, 106)	(50, 151)	(49, 197)	(48, 290)	(47, 372)	
Sets	F1	F2	F3	F4	F5	F6	
(m_q, m_s) (Λ)	(0.20, 0.25)	(0.20, 0.30)	(0.20, 0.45)	(0.20, 0.60)	(0.20, 0.90)	(0.20, 1.2)	
Λ (MeV)	342	340	331	322	311	303	
(m_q, m_s) (MeV)	(68, 86)	(68, 102)	(66, 149)	(64, 193)	(62, 280)	(61, 364)	
Sets	G1	G2	G3	G4	G5	G6	
(m_q, m_s) (Λ)	(0.25, 0.28)	(0.25, 0.30)	(0.25, 0.45)	(0.25, 0.60)	(0.25, 0.90)	(0.25, 1.2)	
Λ (MeV)	337	332	323	320	307	302	
(m_q, m_s) (MeV)	(84, 94)	(83, 99)	(81, 145)	(80, 192)	(77, 276)	(76, 363)	
Sets	H1	H2	H3	H4	H5	H6	
(m_q, m_s) (Λ)	(0.30, 0.45)	(0.30, 0.60)	(0.30, 0.75)	(0.30, 0.90)	(0.30, 1.0)	(0.30, 1.2)	
Λ (MeV)	319	313	308	301	300	296	
(m_q, m_s) (MeV)	(96, 143)	(94, 188)	(92, 231)	(90, 271)	(90, 300)	(89, 355)	

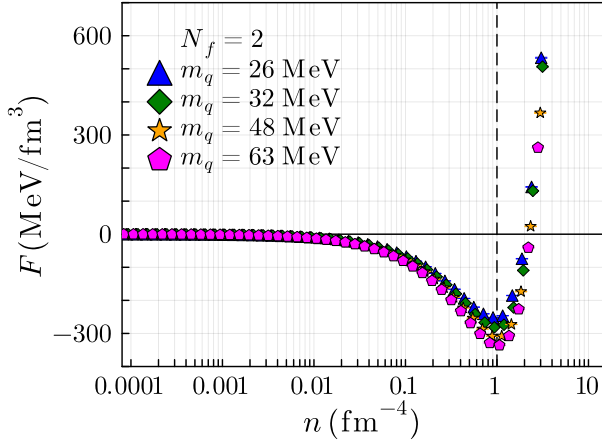


FIG. 1. Instanton density versus free energy computed in ILM with the flavor SU(2) symmetric quarks of the current quark masses, $m_q = 26, 32, 48$ and 63 MeV.

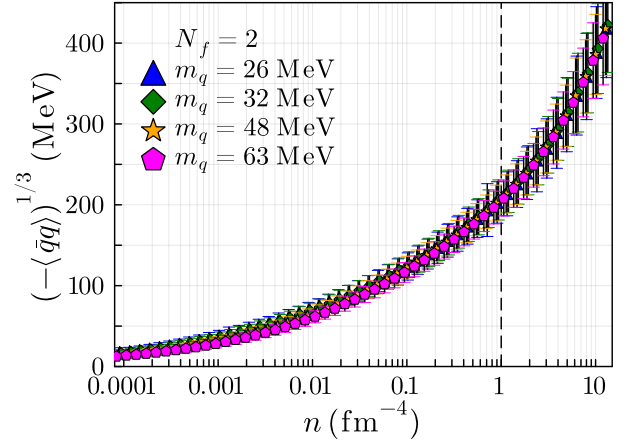


FIG. 2. Instanton density versus cubic root of light quark condensate in magnitude in ILM with the flavor SU(2) symmetric quarks that are equal to those in Fig. 1.

is consistent with the recent evaluation from lattice QCD calculation; $\langle 0|\bar{q}q|0\rangle = (\langle 0|\bar{u}u|0\rangle + \langle 0|\bar{d}d|0\rangle)/2 = -[272(5) \text{ MeV}]^3$ [34] even though our result is slightly underestimated.

In Fig. 3, we show the plot of the dataset $(\langle \bar{q}q \rangle, F)$ computed by the flavor SU(2) symmetric ILM. The results correspond to parameter sets B3 through B6, with associated current quark masses summarized in Table I.

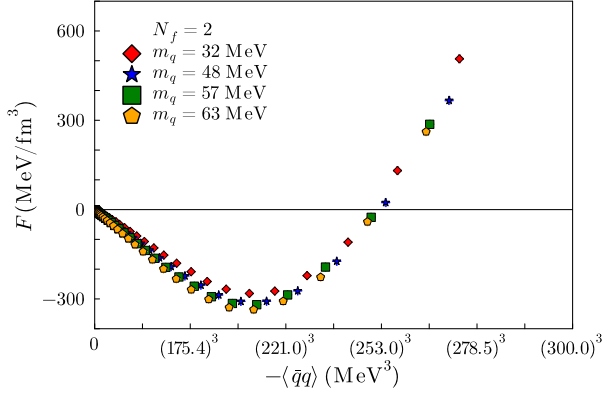


FIG. 3. Scatter plot created using the values of the free energy F and the quark condensate $\langle\bar{q}q\rangle$ calculated by the flavor SU(2) symmetric ILM at each density n , with $\langle\bar{q}q\rangle$ on the horizontal axis and F on the vertical axis. Different marker shapes represent different m_q values.

In all cases, the free energy exhibits a clear minimum at $\langle\bar{q}q\rangle \neq 0$. The finite value of the quark condensate provides direct evidence for the D χ SB in the vacuum. The behavior of F near $\langle\bar{q}q\rangle = 0$ is approximately linear, reflecting the explicit breaking of chiral symmetry due to the finite current quark mass m_q . This linear dependence is consistent with the result from the chiral effective theories in the small quark condensate region.

Performing the polynomial regression on the dataset $(\langle\bar{q}q\rangle, F)$, we obtain the curvature at each quark mass m_q . For instance, we evaluate the curvature as $C_2 = -7.73 \times 10^{-5} \text{ MeV}^{-2}$ at the light quark mass of $m_q = 0.08 \Lambda = 26 \text{ MeV}$ by using the polynomial model of order $k = 3$. Figure 4 shows the curvature evaluated at each current quark mass m_q in the flavor SU(2) symmetric ILM. Across the entire range $17 \text{ MeV} < m_q < 63 \text{ MeV}$, we observe that C_2 remains negative, which contrasts with our previous results obtained in the flavor SU(3) symmetric case [17], shown as red stars in Fig. 4 where C_2 is positive.

This difference in signs indicate a qualitative change in the type of D χ SB between the flavor SU(2) and SU(3) symmetric cases. The negative curvature implies that the ordinary type of D χ SB occurs in the vacuum for the flavor SU(2) symmetric case according to our criterion.

B. The (2+1)-flavor calculation

Figure 5 shows the dataset $(\langle\bar{q}q\rangle, F)$ computed in ILM with the (2+1)-flavor quarks. In this plot, the light quark mass m_q is fixed at 0.1Λ , while the strange quark mass m_s is varied in the range $0.15 \Lambda \leq m_s \leq 1.2 \Lambda$ (see Table II).

For all simulations at different quark masses, the free energy exhibits a minimum at a finite value of $\langle\bar{q}q\rangle$, indicating that D χ SB occurs also in the vacuum of the

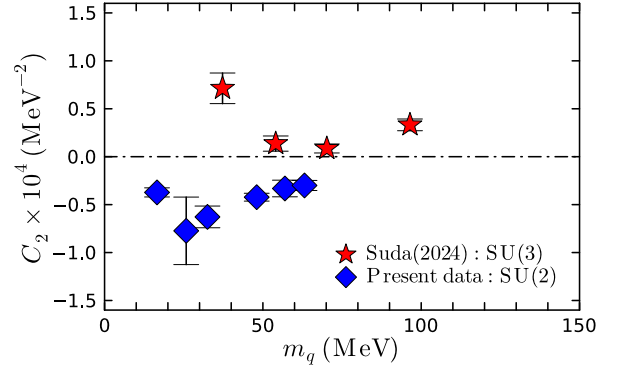


FIG. 4. Curvature C_2 evaluated in the flavor SU(2) symmetric ILM for different quark masses are shown by blue diamonds, which corresponding to Sets B1-B6. The flavor SU(3) results are presented with red stars from our previous study [17].

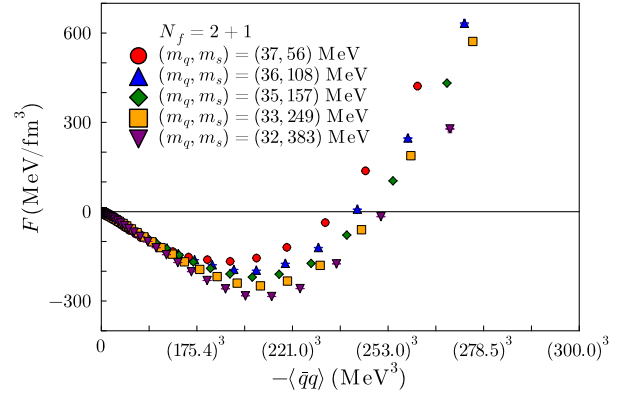


FIG. 5. The free energy versus the quark condensate computed in ILM with the (2+1)-flavor dynamical quarks masses, corresponding to Sets D1, D2, D3, D5 and D7.

(2+1)-flavor ILM. As m_s increases, the free energy minimum becomes deeper and the magnitude of the quark condensate at the minimum becomes larger. This trend closely resembles the behavior observed in the flavor SU(3) ILM [17], suggesting that the strange quark mass slightly increases the absolute value of the quark condensate.

Figure 6 shows the curvature C_2 evaluated in ILM with the (2+1)-flavor quarks. Panels (a)-(e) correspond to different light quark masses m_q , and illustrate that C_2 is positive when the strange quark mass m_s is smaller than 57-192 MeV, but becomes negative as m_s exceeds these values.

These results suggest that ILM exhibits anomaly-driven type of D χ SB in the nearly flavor SU(3) symmetric regime, characterized by positive curvature. In contrast, as the mass difference between the light and strange quarks increases, that is, as the system moves away from the flavor SU(3) symmetric limit, the system

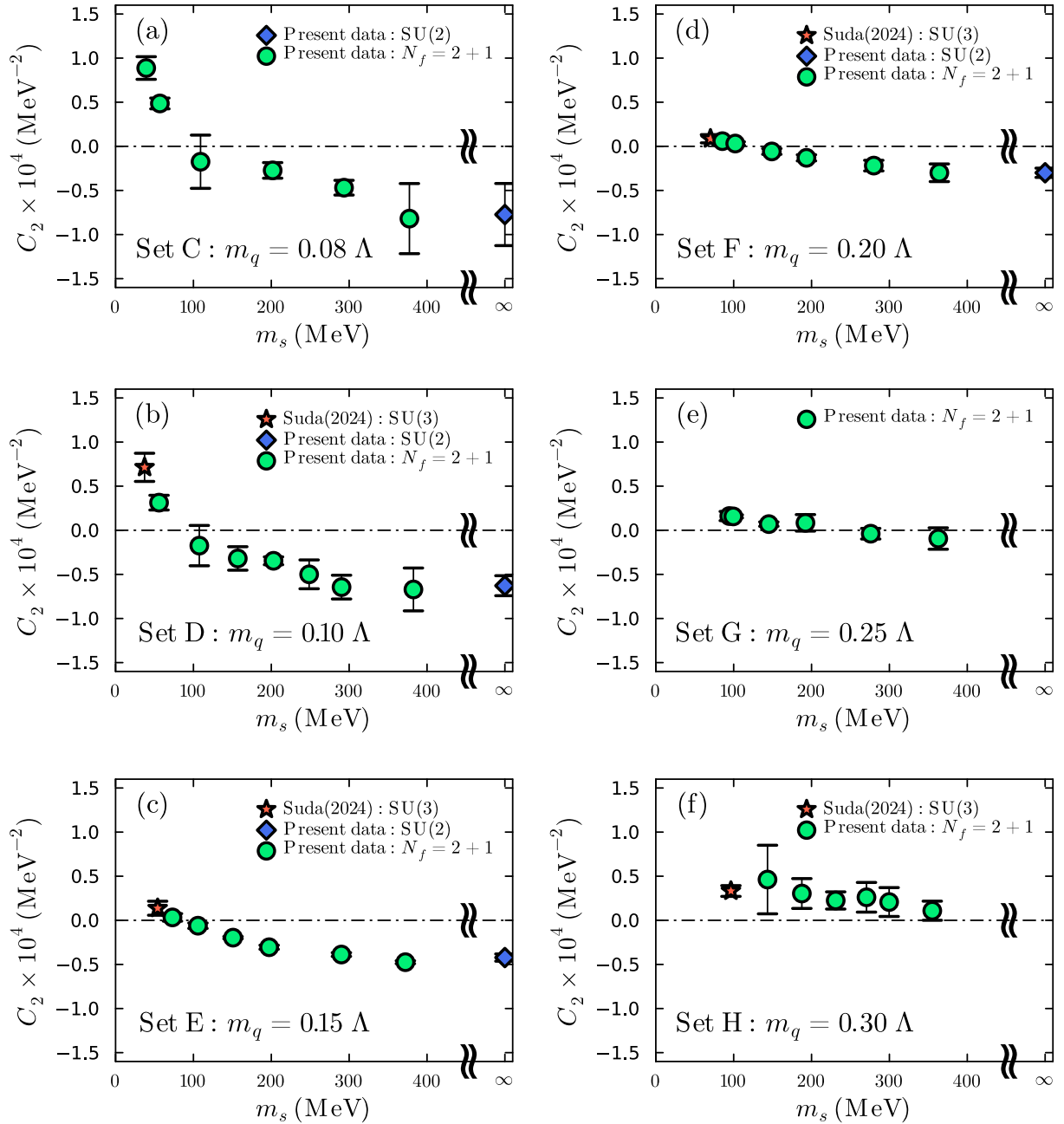


FIG. 6. Plots of m_s versus C_2 that is evaluated by IILM with the (2+1)-flavor quarks of Sets C-H. The values of C_2 are obtained by polynomial regression of degree $k = 3$. The results of the flavor SU(3) symmetric calculation in our previous study [17] are presented with red stars for $m_q = 0.10, 0.15, 0.20$ and 0.30Λ . The results of the flavor SU(2) symmetric calculation are presented with blue diamonds for $m_q = 0.08, 0.10, 0.15$ and 0.20Λ on the point of $m_s = \infty$.

tends to favor the ordinary type of D χ SB, indicated by negative curvature.

When the light quark mass is relatively heavy, such as $m_q = 0.3 \Lambda$ shown in panel (f), the curvature remains positive across the full range of m_s . This result is consistent with the observation that the curvature is positive in the nearly flavor SU(3) symmetric case explained above. In fact, in panel (f), the light quark mass is fixed at

$m_q = 0.3 \Lambda$, and the rightmost data point corresponds to the case with the heaviest s quark mass, $m_s = 1.2 \Lambda$. The mass ratio in this case is $m_s/m_q = 4.0$. On the other hand, the third data point from the left in panel (a) corresponds to $m_q = 0.08 \Lambda$ and $m_s = 0.30 \Lambda$, yielding a similar ratio $m_s/m_q = 3.75$. From the viewpoint of the flavor SU(3) symmetry breaking characterized by the mass ratio m_s/m_q , the result in panel (f) should be

compared with the left three data points in panel (a). In both cases, the curvature is positive within error, indicating that the results are consistent. This observation motivates us to study the dependence of the curvature on the mass ratio m_s/m_q , addressed in the next section.

C. Comparison among the flavor SU(2), SU(3) symmetric and (2+1)-flavor calculations

In Fig. 6, we have compared the curvature C_2 calculated in the (2+1)-flavor IILM with those obtained in the flavor SU(3) and SU(2) symmetric cases. As the strange quark mass m_s increases, the curvature smoothly decreases from a positive value that is characteristic of anomaly-driven type of D χ SB to a negative value defining the ordinary type of D χ SB. This can be seen in the change from the flavor SU(3) symmetric calculation to the flavor SU(2) symmetric case that is mediated by the (2+1)-flavor calculations. This trend is clearly observed in the results for $m_q = 0.10, 0.15$, and 0.20Λ , corresponding to panels (b), (c), and (d) of Fig. 6. Although the degree of decrease becomes more gradual for heavier values of m_q , the qualitative behavior—namely, the decrease in curvature with increasing m_s —is consistently seen across all values of m_q .

These observations support our conjecture that IILM with nearly flavor SU(3) symmetric quark masses exhibits the anomaly-driven type of D χ SB, whereas it tends to favor the ordinary type when the flavor SU(3) symmetry is explicitly broken by mass difference between the light and strange quarks.

Figure 7 shows the dependence of the curvature C_2 on the ratio of strange to light quark masses, m_s/m_q . The flavor SU(3) and SU(2) symmetric results correspond to $m_s/m_q = 1$ and $m_s/m_q \rightarrow \infty$, respectively, while the (2+1)-flavor calculations cover the intermediate region $1 < m_s/m_q \leq 15$ in the present study.

We clearly observe that C_2 decreases as the ratio increases, regardless of the absolute value of m_q . Figure. 7 suggests that the curvature changes its sign from positive to negative around $m_s/m_q \sim 3$, and given this result, it is expected to become negative at the physical point $m_s/m_q = 27.3$. In the limit of $m_s/m_q \rightarrow \infty$, the curvature eventually approaches negative value suggested by the results of the flavor SU(2) symmetric calculation.

These results suggest that the anomaly-driven type of D χ SB is favored only within a narrow region where the flavor SU(3) symmetry is approximately realized. Once this symmetry is broken by a mass difference among the u , d , and s quarks, the system is expected to realize the ordinary type of D χ SB in the vacuum.

Figure 8 summarizes the distribution of the simulations at different quark masses computed in this study in the plane of m_q and m_s . In this figure, each marker corresponds to specific quark masses: the flavor SU(3) symmetric calculations are plotted with star, the flavor SU(2) symmetric calculations are denoted by diamond,

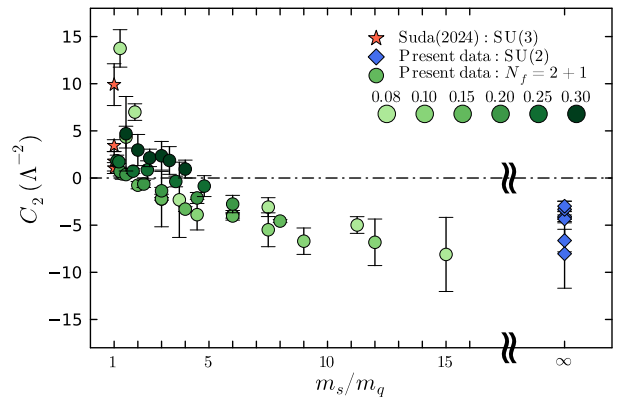


FIG. 7. m_s -to- m_q ratio dependence of C_2 . The results of C_2 in the flavor SU(3) and SU(2) symmetric and the (2+1)-flavor calculations are presented by red star, blue diamond and green circle, respectively. For the (2+1)-flavor results, the results with same m_q in units of Λ are filled with same green gradation.

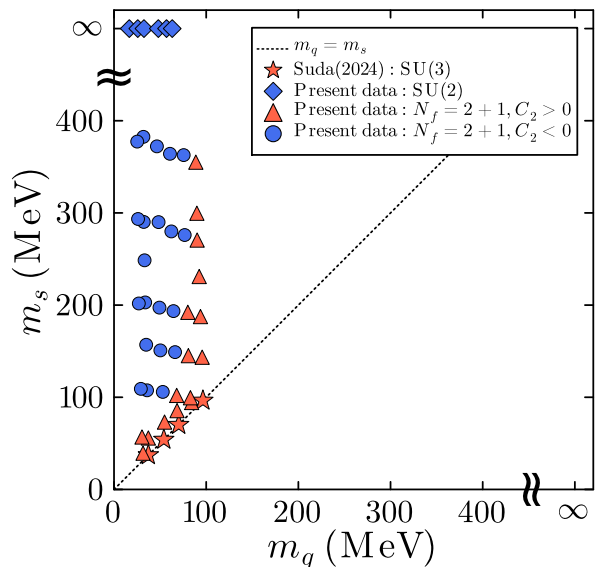


FIG. 8. Our simulation points in the plane of m_q and m_s . Points corresponding to the flavor SU(2) symmetric calculations are symbolically located on the axis $m_s = \infty$.

and the (2+1)-flavor calculations with a positive and a negative curvature are shown with triangle and circle, respectively. The flavor SU(3) symmetric and a part of the (2+1)-flavor calculations with triangle marker have a positive curvature, associated with the anomaly-driven type of D χ SB. While the flavor SU(2) symmetry and a part of the (2+1)-flavor calculations with circle marker have a negative curvature, corresponding to the ordinary type of D χ SB.

In the region where $m_q < 80$ MeV, we observe that the markers with a positive curvature are clustered just

above the flavor SU(3) symmetric line, $m_q = m_s$. This suggests that the anomaly-driven type of D χ SB can still occur even when the flavor SU(3) symmetry is slightly broken. However, as m_s increases to around 80 MeV with keeping m_q fixed below this value, the markers with a negative curvature appear, indicating a change in the type of D χ SB from the anomaly-driven to the ordinary.

These results further support our expectation that the anomaly-driven type of D χ SB is realized only in the vicinity of the flavor SU(3) symmetry, while even a small breaking of this symmetry favors the ordinary type.

IV. CONCLUSIONS

In this study, we have investigated the type of dynamical chiral symmetry breaking (D χ SB) using the interacting instanton liquid model (IILM) with the flavor SU(2) symmetric and (2+1)-flavor quarks. Following our previous work [17], we defined the type of D χ SB based on the sign of the second derivative of the free energy with respect to the quark condensate at the origin.

Our calculations show that in the flavor SU(2) symmetric case the curvature is negative. A negative curvature means the realization of the ordinary type of D χ SB by our criterion. This contrasts with the results of a positive curvature obtained in the flavor SU(3) symmetric calculation [17]. This difference can be understood in terms of the 't Hooft vertex induced by instantons. The quark determinant part in the partition function corresponds to the 't Hooft vertex and it generates an effective $2N_f$ -quark interaction. In the flavor SU(2) symmetric calculation, this part yields a four-quark interaction, which does not play the same role as the KMT term. This means that the axial anomaly contribution represented as a six-quark interaction is absent in this case. Thus, the ordinary type of D χ SB is realized in the flavor SU(2) symmetric IILM. In contrast, in the flavor SU(3) symmetric IILM, the quark determinant part corresponds to the 't Hooft vertex with a six-quark interaction. This is consistent with the KMT term responsible for the axial anomaly. Therefore, the anomaly-driven type of D χ SB is realized in the flavor SU(3) symmetric case.

In the (2+1)-flavor calculations, we have found that the curvature decreases as the strange quark mass increases and eventually becomes negative. As we increase the strange quark mass, the (2+1)-flavor calculation effectively changes from the flavor SU(3) symmetric calculation to the flavor SU(2) symmetric one. In this change, we have observed that when the strange quark mass exceeds approximately three times those of the light quarks, the curvature turns negative. This implies that the anomaly-driven type of D χ SB, characterized by a positive curvature, realizes for a small ratio of m_s/m_q , while the ordinary type of D χ SB occurs with a large ratio.

Our findings suggest that the magnitude of the strange quark mass plays a crucial role in determining the domi-

nant chiral symmetry breaking mechanism. When the ratio m_s/m_q is near one, the system retains the (approximate) flavor SU(3) symmetry. In this case, the six-quark interaction exists and incorporates the axial anomaly. Thus, the anomaly-driven type of D χ SB is realized. As the strange quark mass increases, the flavor SU(3) symmetry is broken, and the strange quark effectively decouples from the system. As a result, the six-quark interaction reduces to a four-quark one. This means the contribution of the axial anomaly induced by the six-quark interaction weakens and thus the ordinary type of D χ SB emerges.

It is interesting direction to investigate how the competition between the flavor SU(3) symmetry breaking and the effects of the $U(1)_A$ anomaly realizes in the hadron spectrum using the chiral effective theories that includes the 't Hooft vertex [35, 36].

The present results may be relevant to recent discussions regarding the nature of the chiral phase transition at finite temperature, whether it is of first order or second order, depending on the number of quark flavors and the role of the axial anomaly [37–39]. However, our current study focuses on the mechanism responsible for chiral symmetry breaking already realized at zero temperature, and a detailed investigation of its relation to finite-temperature phenomena is left for future work.

In order to obtain the clue to the understanding of the QCD vacuum structure, we desire information about the regions where the quark masses are lighter than present values. To make the quark mass light, we need to enlarge the simulation box size while keeping the instanton density fixed to ensure the validity of treating the light quarks. Achieving this requires the increasing the total number of instantons and anti-instantons in the simulation, which in turn demands more computational resources. This will be addressed in future work.

ACKNOWLEDGMENTS

This work of Y.S. was supported by JST SPRING, Japan Grant Number JPMJSP2106 and JPMJSP2180. The work of D.J. was supported in part by Grants-in-Aid for Scientific Research from JSPS (JP21K03530, JP22H04917, JP23K03427 and JP25K07315).

Appendix A: Semiclassical instanton amplitude

In this study, we use the semiclassical instanton amplitude $f(\rho)$ with up to two-loop β functions [13]. The

explicit form is given by

$$f(\rho) = C_{N_c} \left[\frac{8\pi^2}{g^2(\rho)} \right]^{2N_c} \exp \left[-\frac{8\pi^2}{g^2(\rho)} \right] \frac{1}{\rho^5} \\ = C_{N_c} \frac{1}{\rho^5} \beta_1(\rho)^{2N_c} \\ \times \exp \left[-\beta_2(\rho) + \left(2N_c - \frac{b'}{2b} \right) \frac{b'}{2b} \frac{1}{\beta_1(\rho)} \ln \beta_1(\rho) \right], \quad (\text{A1})$$

$$C_{N_c} = \frac{0.466e^{-1.679N_c}}{(N_c - 1)!(N_c - 2)!}, \quad (\text{A2})$$

where the gauge coupling g^2 is given as a function of the instanton size ρ ; the β functions β_1, β_2 include up to two-loop order; and the Gell-Mann–Low coefficients are given as follows:

$$\beta_1(\rho) = -b \ln(\rho\Lambda), \quad \beta_2(\rho) = \beta_1(\rho) + \frac{b'}{2b} \ln \left[\frac{2}{b} \beta_1(\rho) \right], \quad (\text{A3})$$

$$b = \frac{11}{3}N_c - \frac{2}{3}N_f, \quad b' = \frac{34}{3}N_c^2 - \frac{13}{3}N_cN_f + \frac{N_f}{N_c}. \quad (\text{A4})$$

Here, the number of colors and flavors are denoted as N_c and N_f . Λ is the scala parameter described in the text.

Appendix B: Explicit expression of the interactions

The explicit expression of $S_{\text{int}}^{(2)}(l, m)$ is given by

$$S_{\text{int}}^{(2)}(l, m) = \begin{cases} S_{IA}^{(2)} + S_{\text{core}}^{(2)} & \text{for } (l, m) = (I, A) \text{ or } (A, I) \\ S_{\text{core}}^{(2)} & \text{for } (l, m) = (I, I) \text{ or } (A, A) \end{cases}, \quad (\text{B1})$$

where I, A denote the instanton and anti-instanton, respectively. $S_{IA}^{(2)}$ is the two-body action that is calculated by using the streamline configuration [27], and $S_{\text{core}}^{(2)}$ represents the phenomenological repulsive core at the short

distance. Their explicit forms are derived in Ref. [26] as

$$\frac{S_{IA}^{(2)}}{S_0} = \frac{1}{(\lambda^2 - 1)^3} \left\{ -4[1 - \lambda^4 + 4\lambda^2 \ln(\lambda)](|u|^2 - 4|u \cdot \hat{R}|^2) \right. \\ \left. + 2[1 - \lambda^2 + (1 + \lambda^2) \ln(\lambda)] \right. \\ \left. \times [(|u|^2 - 4|u \cdot \hat{R}|^2)^2 + |u|^4 + 2(u^*)^2(u^*)^2] \right\}, \quad (\text{B2})$$

$$\frac{S_{\text{core}}^{(2)}}{S_0} = \frac{A}{\lambda^4} |u|^2, \quad (\text{B3})$$

where the single instanton action is calculated as $S_0 = 8\pi^2/g^2(\rho) = \beta_1(\bar{\rho})$ with $\bar{\rho} \equiv \sqrt{\rho I \rho A}$. The parameter λ , called as the conformal parameter, is introduced in construction of the streamline ansatz [40], given by

$$\lambda = \frac{1}{2} \frac{R^2 + \rho_l^2 + \rho_m^2}{\rho_l \rho_m} + \frac{1}{2} \sqrt{\frac{(R^2 + \rho_l^2 + \rho_m^2)^2}{\rho_l^2 \rho_m^2} - 4}, \quad (\text{B4})$$

with $R_\mu = z_{l,\mu} - z_{m,\mu}$ and $R^2 = R_\mu R_\mu$ ($\mu = 1, 2, 3, 4$). \hat{R}_μ is a unit vector of R_μ . The four-vector u_μ characterizes the relative color orientation between instantons of color degrees of freedom U_l and U_m , given by

$$u_\mu = \frac{1}{2i} \text{Tr}(U_l^\dagger U_m \tau_\mu^+), \quad (\text{B5})$$

with the four dimensional Pauli matrix $\tau_\mu^\pm = (\tau_i, \mp i\mathbf{1}_2)$. With those vectors, the inner product $(u \cdot \hat{R})$ is understood as a contraction: $(u \cdot \hat{R}) = \sum_{\mu=1}^4 u_\mu \hat{R}_\mu$.

The overlap matrix T has the structure of

$$T = \begin{pmatrix} \mathbf{0}_{N_+ \times N_+} & (\mathcal{T})_{N_+ \times N_-} \\ (\mathcal{T})_{N_- \times N_+} & \mathbf{0}_{N_- \times N_-} \end{pmatrix}, \quad (\text{B6})$$

with the matrix element

$$(\mathcal{T})_{IJ} = \int d^4x \psi_{0,I}^*(x; U, \rho, z) i\gamma_\mu D_\mu \psi_{0,J}(x; U, \rho, z). \quad (\text{B7})$$

Since we only consider the system with $N_+ = N_-$, the overlap matrix is square. The explicit expression of matrix element in Eq. (B7) is given in Ref. [26, 41] as

$$(\mathcal{T})_{IJ} = i(u \cdot \hat{R}) \frac{1}{\sqrt{\rho I \rho J}} F(\lambda), \quad (\text{B8})$$

$$F(\lambda) = 6 \int_0^\infty \frac{r^{3/2}}{(r + 1/\lambda)^{3/2} (r + \lambda)^{5/2}} dr \\ \approx \frac{c_2 \lambda^{3/2}}{[1 + 1.25(\lambda^2 - 1) + c_2(\lambda^2 - 1)^2]^{3/4}}, \quad (\text{B9})$$

with $c_1 = 3\pi/8$ and $c_2 = (3\pi/32)^{4/3}$.

- [2] S. Adler, “Axial-Vector Vertex in Spinor Electrodynamics,” *Phys. Rev.* **177**, 2426 (1969).
- [3] J. S. Bell and R. Jackiw, “PCAC puzzle: $\pi^0 \rightarrow \gamma\gamma$ in σ model,” *Nuovo Cimento A* **60**, 47 (1969).
- [4] S. D. Bass and P. Moskal, “ η' and η mesons with connection to anomalous glue,” *Rev. Mod. Phys.* **91**, 015003 (2019).
- [5] S. Weinberg, “Phenomenological Lagrangians,” *Physica* **96A**, 327 (1979).
- [6] J. Gasser, H. Leutwyler, “Chiral perturbation theory: expansions in the mass of the strange quark,” *Nucl. Phys. B* **250**, 465 (1985).
- [7] Y. Nambu, G. Jona-Lasinio, “Dynamical Model of Elementary Particles Based on an Analogy with Superconductivity. I,” *Phys. Rev.* **122**, 345 (1961).
- [8] M. Gell-Mann, M. Lévy, “The axial vector current in beta decay,” *Nuovo. Cim.* **16**, 705 (1960).
- [9] S. Kono, D. Jido, Y. Kuroda, and M. Harada, “The role of $U_A(1)$ breaking term in dynamical chiral symmetry breaking of chiral effective theories,” *PTEP* **2021**, no. 9, 093D02 (2021).
- [10] M. Kobayashi and T. Maskawa, “Chiral symmetry and η - X mixing,” *Prog. Theor. Phys.* **44**, 1422 (1970).
- [11] M. Kobayashi, H. Kondo, and T. Maskawa, “Symmetry breaking of the chiral $U(3) \otimes U(3)$ and the quark model,” *Prog. Theor. Phys.* **45**, 1955 (1971).
- [12] G. 't Hooft, “Symmetry breaking through Bell–Jackiw anomalies,” *Phys. Rev. Lett.* **37** (1976) 8.
- [13] G. 't Hooft, “Computation of the quantum effects due to four-dimensional pseudoparticle,” *Phys. Rev. D* **14**, 3432 (1976).
- [14] C. Rosenzweig, J. Schechter, and C. G. Trahern, “Is the effective Lagrangian for quantum chromodynamics a σ model?,” *Phys. Rev. D* **21**, 3388 (1980).
- [15] P. Di Vecchia and G. Veneziano, “Chiral dynamics in the large N limit,” *Nucl. Phys. B* **171**, 253 (1980).
- [16] E. Witten, “Large N chiral dynamics,” *Ann. Phys.* **128**, 363 (1980).
- [17] Y. Suda and D. Jido, “Possible scenario of dynamical chiral symmetry breaking in the interacting instanton liquid model,” *Phys. Rev. D* **110**, 014037 (2024).
- [18] C. G. Callan, R. Dashen, and D. J. Gross, “Toward a theory of the strong interactions,” *Phys. Rev. D* **17**, 2717 (1978).
- [19] C. G. Callan, R. Dashen, and D. J. Gross, “A theory of hadronic structure,” *Phys. Rev. D* **19**, 1826 (1979).
- [20] M. A. Shifman, A.I. Vainshtein, V.I. Zakharov, “Instanton density in a theory with massless quarks,” *Nucl. Phys. B* **163**, 46 (1980).
- [21] S. Navas, *et al.*, (Particle Data Group), “Review of Particle Physics,” *Phys. Rev. D* **110**, 030001 (2024).
- [22] E. V. Shuryak, “The role of instantons in quantum chromodynamics: (I). Physical vacuum,” *Nucl. Phys. B* **203**, 93 (1982).
- [23] E. V. Shuryak, “The role of instantons in quantum chromodynamics: (II). Hadronic structure,” *Nucl. Phys. B* **203**, 116 (1982).
- [24] C. Bernard, “Gauge zero modes, instanton determinants, and quantum-chromodynamic calculations,” *Phys. Rev. D* **19**, 3013 (1979).
- [25] D. I. Dyakonov, and V. Yu. Petrov, “A theory of light quarks in the instanton vacuum,” *Nucl. Phys. B* **272**, 457 (1986).
- [26] T. Schäfer and E. V. Shuryak, “Interacting instanton liquid model in QCD at zero and finite temperature,” *Phys. Rev. D* **53**, 6522 (1996).
- [27] J. J. M. Verbaarschot, “Streamlines and conformal invariance in Yang-Mills theories,” *Nucl. Phys. B* **362**, 33 (1991).
- [28] T. Schäfer and E. V. Shuryak, “Instantons in QCD,” *Rev. Mod. Phys.* **70**, 323 (1998).
- [29] N. Metropolis, A. W. Rosenbluth, M. N. Rosenbluth, A. H. Teller, E. Teller, “Equation of state calculations by fast computing machines” *J. Chem. Phys.* **21**, 1087 (1953).
- [30] S. Duane, A. D. Kennedy, B. J. Pendleton, D. Roweth, “Hybrid Monte Carlo” *Phys. Lett. B* **195**, 2 (1975).
- [31] K. Binder and D. Herrmann, “Monte Carlo Simulations in Statistical Physics An Introduction (6th ed.),” Springer Berlin, Heidelberg (2010).
- [32] D. Randau and K. Binder, “A Guide to Monte Carlo Simulations in Statistical Physics,” Cambridge Univ. Press. (2014).
- [33] M. Hanada, “Markov Chain Monte Carlo for Dummies,” arXiv:1808.08490.
- [34] P. Gubler and D. Satow, “Recent progress in QCD condensate evaluations and sum rules,” *Prog. Part. Nucl. Phys.* **106**, 1 (2019).
- [35] Y. Kuroda, M. Harada, S. Matsuzaki, and D. Jido, “Inverse mass hierarchy of light scalar mesons driven by anomaly-induced flavor breaking,” *Prog. Theor. Exp. Phys.* **2020**, 053D02 (2020).
- [36] T. Saionji, D. Jido, and M. Harada, “Inverse mass ordering of light scalar mesons in the Nambu–Jona-Lasinio model,” *Prog. Theor. Exp. Phys.* **2023**, 033D01 (2023).
- [37] R. D. Pisarski and F. Rennecke, “Conjectures about the Chiral Phase Transition in QCD from Anomalous Multi-Instanton Interactions,” *Phys. Rev. Lett.* **132**, 251903 (2024).
- [38] G. Fejos and T. Hatsuda, “Order of the $SU(N_f) \times SU(N_f)$ chiral transition via the functional renormalization group,” *Phys. Rev. D* **110**, 016021 (2024).
- [39] F. Giacosa, G. Kovács, P. Kovács, R. D. Pisarski, and F. Rennecke, “Anomalous $U(1)_A$ couplings and the Columbia plot,” *Phys. Rev. D* **111**, 016014 (2025).
- [40] A. V. Yung, “Instanton vacuum in supersymmetric QCD,” *Nucl. Phys. B* **297**, 47 (1988).
- [41] E. V. Shuryak and J. J. M. Verbaarschot, “Baryon number violation and nonperturbative weak processes at superconducting super collider energies,” *Phys. Rev. Lett.* **68**, 2576 (1992).